

Joint Lossless Compression and Steganography for Medical Images via Large Language Models

Pengcheng Zheng¹, Xiaorong Pu^{1,2}, Kecheng Chen³, Jiaxin Huang⁴, Meng Yang¹, Bai Feng²,
Yazhou Ren^{1,2}, Jianan Jiang¹

¹School of Computer Science and Engineering, University of Electronic Science and Technology of China, Chengdu, China

²Shenzhen Institute for Advanced Study, University of Electronic Science and Technology of China, Shenzhen, China

³Department of Electrical Engineering and the Centre for Intelligent Multidimensional Data Analysis (CIMDA), City University of Hong Kong

⁴Mohamed bin Zayed University of Artificial Intelligence

zpc777@std.uestc.edu.cn, puxiaor@uestc.edu.cn, cs.ckc96@gmail.com, hjx1134@gmail.com, cdtu.daoshan@gmail.com,
bai.liruxz.ai@gmail.com, yazhou.ren@uestc.edu.cn, 202521080616@std.uestc.edu.cn

Abstract

Recently, large language models (LLMs) have driven promising progress in lossless image compression. However, directly adopting existing paradigms for medical images suffers from an unsatisfactory trade-off between compression performance and efficiency. Moreover, existing LLM-based compressors often overlook the security of the compression process, which is critical in modern medical scenarios. To this end, we propose a novel joint lossless compression and steganography framework. Inspired by bit plane slicing (BPS), we find it feasible to securely embed privacy messages into medical images in an invisible manner. Based on this insight, an adaptive modalities decomposition strategy is first devised to partition the entire image into two segments, providing global and local modalities for subsequent dual-path lossless compression. During this dual-path stage, we innovatively propose a segmented message steganography algorithm within the local modality path to ensure the security of the compression process. Coupled with the proposed anatomical priors-based low-rank adaptation (A-LoRA) fine-tuning strategy, extensive experimental results demonstrate the superiority of our proposed method in terms of compression ratios, efficiency, and security. The source code will be made publicly available.

Introduction

Image compression task aims to reduce image size as much as possible, making it essential for high-quality data storage and transmission. Driven by the advancement of deep neural networks (DNNs), there has been remarkable progress in image compression, including lossy and lossless codecs (Li et al. 2025; Zheng and Gao 2024; Cai et al. 2024; Mao et al. 2025; Lu et al. 2025; Zheng et al. 2023). Although existing lossy compression methods have shown remarkable performance for natural images, lossless compression for medical images has attracted massive attention from the medical imaging community, as even subtle degradations (e.g., mild blurring of tissues or organs) may compromise diagnostic accuracy (Zhang et al. 2024b; Liu et al. 2024; Zheng et al. 2025).

Copyright © 2025, Association for the Advancement of Artificial Intelligence (www.aaai.org). All rights reserved.

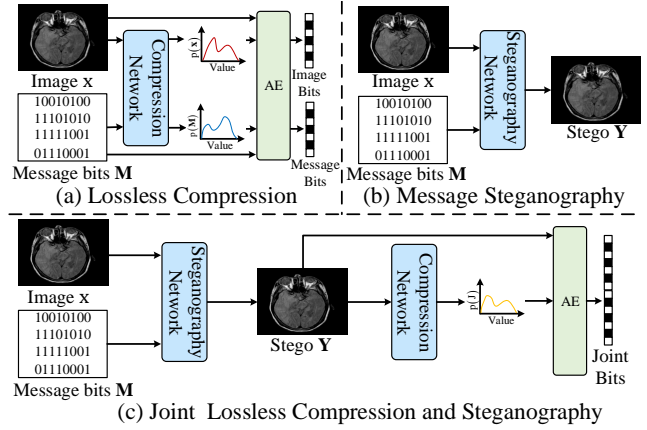


Figure 1: Standard Lossless Compression and Steganography vs. our proposed joint framework.

Recently, large language models (LLMs) have shown great success in probabilistic modeling and lossless compression (Chen et al. 2024b; Du et al. 2025; Chen et al. 2024a). This is own to the so-called philosophy, “*Intelligence*” and “*Compression*” are two sides of the same coin (MacKay 2003). Theoretically, minimizing the negative log-likelihood loss for next-token prediction is equivalent to maximizing the lossless compression objective (Heurtel-Depeiges et al. 2024). Meanwhile, entropy coding in lossless compression seeks to accurately model data distribution to minimize the coding bitrate (Mao, Pirk, and Xue 2025; Valmeekam et al. 2023; Zhang et al. 2023, 2024a; Wang et al. 2025). Consequently, LLMs could potentially provide an accurate probability distribution of images for entropy coding (e.g., arithmetic coding). Recently, this perspective is supported by Delétang et al. (2024) (Delétang et al. 2024) who leverages the pre-trained LLMs to achieve competitive lossless compression ratios across various modalities, including text, audio and images. Whereas it can beat some domain-specific compressors by leveraging LLMs’ unprecedented intelligence, its encoding and decoding time are much slower than other baselines due to the inherent down-

side of autoregressive models. Compared to autoregressive paradigm, latent variable models, *e.g.*, variational autoencoder (VAE) often demonstrates impressive inference speed (Pinheiro Cinelli et al. 2021; Child 2021). By utilizing the *bits back* coding framework (Sugiyama, Suzuki, and Matsuda 2024) (predominantly, bits-back ANS), a VAE can be translated into a lossless codec. Whilst it provides an efficient lossless compression method, its compression ratio is always unsatisfactory (Zhou et al. 2018; Jia et al. 2024).

With broad generality, autoregressive models (*e.g.*, LLMs) can often be the most powerful but the slowest, while variational autoencoders are often the weakest but the fastest (Tian et al. 2024; Child 2021; An et al. 2024). To this end, a potential option to address the above-mentioned issue is the combined use of autoregressive and latent variable models, achieving a great trade-off between compression performance and inference speed. Although existing combined methods (Zhang et al. 2024b; Kang et al. 2022) enable the efficient capture of both global and local data modalities, we argue that scaling them to the medical lossless image compression task is still unsatisfactory. First, these methods usually ignore the security of compressing medical images, where abundant meta information is attached to the images, *e.g.*, patients’ name, gender, ID number, and symptoms. For example, the DICOM standard (Varma 2012) separately compresses image and its meta information, putting patients’ privacy at huge risk of being attacked by hackers when transmitted over the network. Second, most existing combined approaches implicitly learn global and local modalities from images, which makes it infeasible to embed the privacy message into the compression process, as even minimal perturbations of global modalities would change the overall appearance of the image. Third, existing combined methods never attempt to leverage the unprecedented intelligence capacity of LLMs, leading to a compromised compression ratio. *Overall, existing methods struggle with maintaining a trade-off between sufficient compression (intelligence) performance and efficiency, and usually ignore the security for medical scenarios.*

Towards above question, we propose the joint lossless compression and steganography framework (as shown in Figure 1) to ensure the security for compressing medical images, as well as rendering a great trade off between compression performance and efficiency. We empirically conduct a confirmatory experiment on bit plane slicing (Tang et al. 2016) (BPS), which splits images in the bit plane dimension. As shown in Figure 3, we find that the information amount in the image is gradually reducing from the most significant plane (MSP) to the least significant plane (LSP). Therefore, we pose an intuitive question: *can we explicitly partition the image \mathbf{x} into two segments, *i.e.*, global and local modalities via BPS, thereby offering us a feasible way to embed the privacy message into the image in an invisible manner?* Obviously, the answer is affirmative. Specifically, we first devise the adaptive modalities decomposition strategy to partition the entire image using a slicing index, ranging in $\{1, \dots, 8\}$, denoted as s . To this end, the first segment comprises the local modalities, represented as $\mathbf{x}^{1:s}$, while the second segment includes the global modalities, *e.g.*, low-

frequency information, represented as $\mathbf{x}^{s+1:8}$. Second, considering that latent variable models cannot capture local features well, while a local autoregressive model is capable of doing so (Schirrmester et al. 2020; Shannon 1948), we propose the dual-path lossless compression scheme to improve the compression ratio. To be note worthy, a novel segmented message steganography algorithm is designed in the local modality path to ensure a secure compression process for medical images. Finally, a simple yet effective fine-tuning strategy, *i.e.*, anatomical priors-based low-rank adaptation (A-LoRA) is designed to further enhance the compression performance and accelerate the training speed. The embeddings of global modality are served as visual prompt to fine-tune the LLM, which bridges the gap between the textual prior within LLM and visual understanding tasks.

Our main contributions can be summarized as follows:

- To explicitly extract the global and local modalities in medical images, we propose the adaptive modalities decomposition strategy, which lays a strong foundation for dual-path compression and provides a feasible way to embed the privacy message into the compression process.
- A dual-path compression scheme is proposed to render a trade-off between sufficient compression performance and efficiency by leveraging LLM’s unprecedented intelligence (compression) capacity. Specially, we devise a novel segmented message steganography algorithm in the local modality path, which embeds multiple message segments into their corresponding bit planes to ensure the security of the medical image compression process.
- Moreover, an anatomical priors-based low-rank adaptation (A-LoRA) fine-tuning strategy is designed to enhance the compression performance and accelerate the training speed.
- To the best of our knowledge, we are the first to explore the unprecedented intelligence of LLMs for medical images in a joint lossless compression and steganography framework. Extensive experimental results demonstrate the superiority of our proposed method in terms of compression performance, efficiency, and security.

Related Work

Latent Variable Models for Compression

Latent variable models employ deep neural networks (DNNs) to map high-dimensional images into low-dimensional latent variables, integrating the *bits-back* coding framework to render lossless image compression. For instance, L3C (Mentzer et al. 2019) employs DNNs to extract latent variables as auxiliary information for lossless compression. However, the DNN-based transform is difficult to satisfy a tight bound on the maximum reconstruction error of each pixel. Therefore, Bai et al. (Bai et al. 2021) propose a new joint lossy image and residual compression framework for learning lossless compression. However, these methods are under the risk of posterior collapse. To this end, ArIB-BPS (Zhang et al. 2024b) provides different importance for hierarchical latent variables, demonstrating superior compression performance with comparable inference speed.

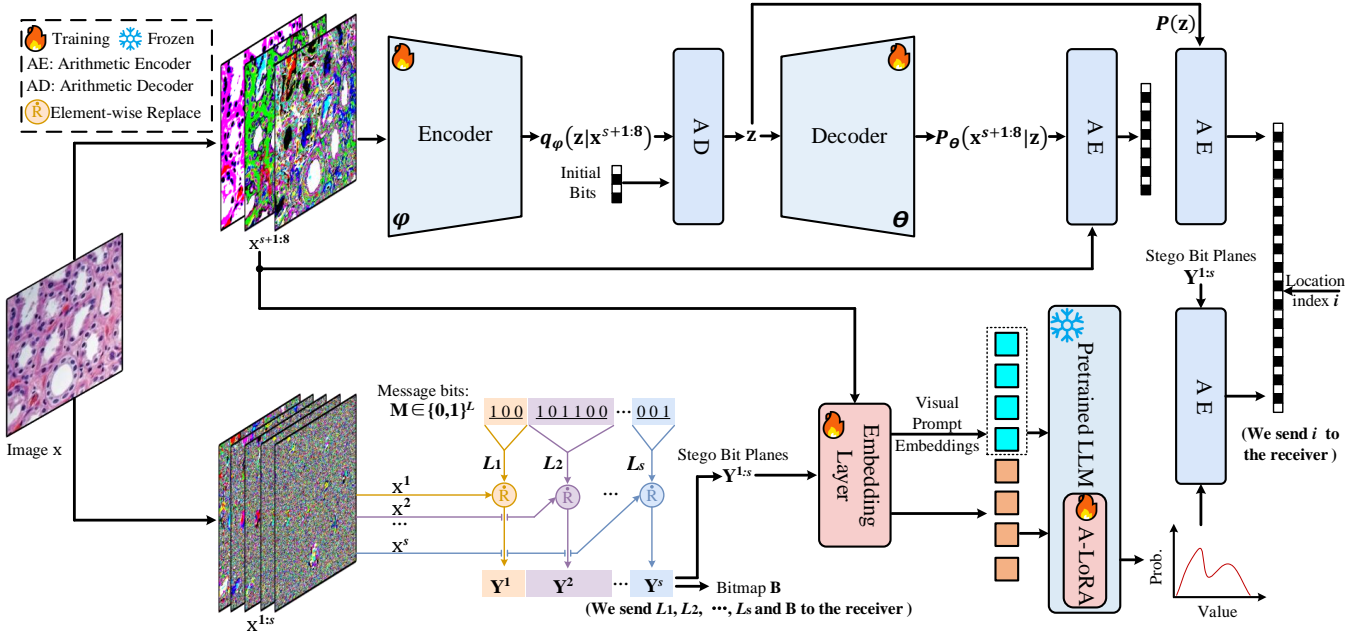


Figure 2: Overview of the proposed framework. In the encoding process, the image is firstly decomposed into global and local modalities via adaptive modalities decomposition strategy. Then, the global modalities are compressed using VAE with *bits-back* coding scheme. The local modalities are compressed by leveraging the unprecedented intelligence of LLM. The final bitstream are concatenated from the dual-path outputs. The decoding order is the reverse of the encoding process.

Nonetheless, latent variable models struggle to capture local features, resulting in suboptimal performance for images with intricate textures, *e.g.*, medical images, where subtle details would significantly influence diagnostic accuracy.

Large Language Models for Compression

LLMs have been widely adopted for computer vision tasks, *e.g.*, image classification and segmentation (Gou et al. 2024; Yang et al. 2023) due to their accurate next token prediction capacity. Recently, literature (Huang et al. 2024) implies the linear growth relation between compression performance and LLM’s intelligence, which provides a new perspective for lossless community. Theoretically, the negative log-loss minimization for the next-token prediction of LLMs is equivalent to optimizing a lossless compression objective. Deletang et al. (Delétang et al. 2024) are pioneered to demonstrate that LLMs, when viewed as compressors, can outperform classical codecs like PNG (Boutell 1997) in lossless compression for images, highlighting their potential in lossless compression community.

To the best of our knowledge, we are the first to leverage the unprecedented intelligence of LLMs in a joint lossless compression and steganography framework for medical images, achieving sufficient compression performance while maintaining security.

Methodology

Preliminary and Overview

Preliminary In this paper, we exploit two paradigms for lossless compression. Latent variable models approximate

the true data distribution $p_{\text{data}}(\mathbf{x})$ with a marginal distribution $p_{\theta}(\mathbf{x})$ defined by

$$p_{\theta}(\mathbf{x}) = \int p_{\theta}(\mathbf{x}, \mathbf{z}) d\mathbf{z} = \int p_{\theta}(\mathbf{x}|\mathbf{z}) p(\mathbf{z}) d\mathbf{z}, \quad (1)$$

where \mathbf{z} is an unobserved latent variable. Since exactly evaluating and optimizing $p_{\theta}(\mathbf{x})$ is intractable, we can rewrite the marginal likelihood $p_{\theta}(\mathbf{x})$ by introducing an *inference model* $q_{\varphi}(\mathbf{z}|\mathbf{x})$:

$$\log p_{\theta}(\mathbf{x}) = \underbrace{\mathbb{E}_{q_{\varphi}(\mathbf{z}|\mathbf{x})} \log \frac{p_{\theta}(\mathbf{x}, \mathbf{z})}{q_{\varphi}(\mathbf{z}|\mathbf{x})}}_{\text{ELBO}(q, \mathbf{x}; \theta, \varphi)} + \underbrace{\mathbb{E}_{q_{\varphi}(\mathbf{z}|\mathbf{x})} \log \frac{q_{\varphi}(\mathbf{z}|\mathbf{x})}{p(\mathbf{z}|\mathbf{x})}}_{=D_{\text{KL}}(q_{\varphi}(\mathbf{z}|\mathbf{x})||p(\mathbf{z}|\mathbf{x}))}. \quad (2)$$

As $D_{\text{KL}}(q_{\varphi}(\mathbf{z}|\mathbf{x})||p(\mathbf{z}|\mathbf{x})) \geq 0$, the inference and generative model can be found by jointly optimizing the Evidence Lower Bound (ELBO) (*i.e.*, maximum $\text{ELBO}(q, \mathbf{x}; \theta, \varphi)$). With the help of the inference network $q_{\varphi}(\mathbf{z}|\mathbf{x})$, it is possible to losslessly compress image \mathbf{x} with *bits back* coding via the following steps. **Step1**: Decode \mathbf{z} with $q_{\varphi}(\mathbf{z}|\mathbf{x})$ from initial bits. **Step2**: Encode \mathbf{x} with $p_{\theta}(\mathbf{x}|\mathbf{z})$. **Step3**: Encode \mathbf{z} with $p(\mathbf{z})$. Proceeding in the reverse order, with the encode and decode operations swapped can losslessly recover the image. Another paradigm is autoregressive models. In this paper, we focus on LLMs, which minimize the negative log-likelihood loss for next-token prediction. As a result, according to the Shannon’s source coding theorem (Yamamoto 1994), the cost of compressing the dataset

$D = \{x_1, x_2, \dots, x_n\}$ can be represented as:

$$\begin{aligned} |S| &= -\log P_f(D) + |f| \\ &= -\sum_{i=1}^n \log p(x_i | x_1, x_2, \dots, x_{i-1}) + |f| \quad (3) \\ &= \mathcal{L}_{LLM} + |f|, \end{aligned}$$

where $|f|$ is the code description of the compression method. Eq. 3 reveals that current LLM training protocols use a maximum-compression objective. It suggests that LLM could potentially serve as a powerful tool for entropy coding, positioning the LLM as a general-purpose compressor for any modality.

Overall Pipelines The overall framework of our proposed lossless image compression pipeline is illustrated in Figure. 2. The original image \mathbf{x} is firstly split into 8-bit planes (as the pixel values of image is in the range of $[0, 255]$), adaptively producing the global modality (significant planes) $\mathbf{x}^{s+1:8}$ and local modality (insignificant planes) $\mathbf{x}^{1:s}$, where s is the slicing index. Subsequently, we compress the global modality via variational autoencoders combined with *bits back* coding scheme. For the local modality, LLM is employed to render an accurate probability representation of each encoded symbol for arithmetic coding. The embeddings of global modality are used as visual prompt for fine-tuning LLM, which bridges the gap between the textual prior within LLM and visual compression tasks. Meanwhile, we introduce a segmented message steganography algorithm when compressing the local modality. Finally, the bitstreams from dual-path are concatenated to generate the final bitstream. The decoding order is the reverse of the encoding process.

Adaptive Modalities Decomposition

The current methods (Chen et al. 2024a; Delétang et al. 2024) compress the entire image with LLM. Although these methods beat classical and learning image compression (LIC)-based codecs by leveraging the unprecedented intelligence within LLM. Their compression efficiency is unsatisfactory due to the inherent downside of autoregressive models. Moreover, they ignore the security when compressing medical images, which is much more urgent for medical scenarios. To this end, it is urgent to render a more efficient and secure compression results for medical images. An intuitive idea is to partition the image into differently significant sub-parts. Specifically, given a image \mathbf{x} with pixel values in the range of $[0, 255]$, we can decompose it into 8-binary bit planes via:

$$\mathbf{x}^l = \lfloor \mathbf{x} / 2^{8-l} \rfloor \bmod 2, \quad (4)$$

where \mathbf{x}^l is the l^{th} bit plane, $\lfloor \mathbf{x} \rfloor$ denotes the largest integer less than or equal to \mathbf{x} . The original image \mathbf{x} can be reconstructed losslessly through the equation:

$$\mathbf{x} = \sum_{l=1}^8 2^{8-l} \times \mathbf{x}^l, \quad (5)$$

As illustrated in Figure 3, the volume of global data modality decreases from the MSP to the LSP. Based on this finding, we adaptively partition the image into global modality

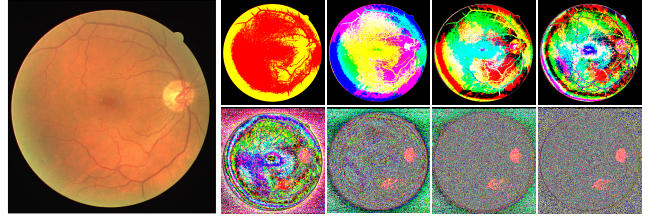


Figure 3: Visualize each bit plane, with the planes organized from the MSP to the LSP, arranged in a left-to-right and top-to-bottom manner.

$\mathbf{x}^{s+1:8}$ and local modality $\mathbf{x}^{1:s}$ with a slicing index s , which can be determined by:

$$s^* = \inf \left(s \mid \sum_{i=1}^s I(\mathbf{x}^i; \mathbf{x}) \geq \beta * I(\mathbf{x}; \mathbf{x}) \right), \quad (6)$$

where $I(\mathbf{x}^i; \mathbf{x})$ denotes the mutual information between the i -th bit plane and the original image, $I(\mathbf{x}; \mathbf{x})$ equals to the entropy of the image \mathbf{x} , *i.e.*, the total information content of the image¹. $\beta \in [0, 1]$ is a hyperparameter controlling information retention (the choice of β is studied in experiment section). \inf is the lower bound, ensuring that when the cumulative mutual information value is greater than the target information value for the first time, s^* is the slicing index.

Dual-Path Lossless Compression

Among all current algorithms, latent variable models are often the weakest but the fastest, while LLM-based models can often be the most powerful but the slowest. As suggested by many previous works (Schirrmeister et al. 2020; Shannon 1948), latent variable models cannot capture local modalities, while LLM-based models are capable of doing so. Thus, an intuitive idea would be to exploit LLM to compress local modalities, and a latent variable model for more global ones. This design can not only achieve a great trade off between model efficiency and performance but also allows us to embed the privacy message into the image in an invisible manner.

Latent Variable Path for Global Modality By recalling the paradigm of latent variable model with *bits back* coding scheme in the preliminary, we compress the global modality via the following steps. **Step1:** Decode \mathbf{z} with $q_\varphi(\mathbf{z} | \mathbf{x}^{s+1:8})$ from initial bits, where initial bits are generated from the auxiliary random source. **Step2:** Encode $\mathbf{x}^{s+1:8}$ with $p_\theta(\mathbf{x}^{s+1:8} | \mathbf{z})$. **Step3:** Encode \mathbf{z} with $p(\mathbf{z})$. The posterior distribution $q_\varphi(\mathbf{z} | \mathbf{x}^{s+1:8})$ and the likelihood probability distribution $p_\theta(\mathbf{x}^{s+1:8} | \mathbf{z})$ are predicted by the residual block based encoder parameterized by φ and the residual block based decoder parameterized by θ , respectively. The decompression order is the reverse of the compression process, *i.e.*, **Step1:** decode \mathbf{z} with $p(\mathbf{z})$. **Step2:** decode $\mathbf{x}^{s+1:8}$ with $p_\theta(\mathbf{x}^{s+1:8} | \mathbf{z})$. **Step3:** Encode \mathbf{z} with $q_\varphi(\mathbf{z} | \mathbf{x}^{s+1:8})$.

LLM Path for Local Modality Since the information of local modality is relatively insignificant, modifying it will

¹We give a detailed proof in the [supplementary material](#).

generally not affect the overall appearance of the image. To achieve an invisible and more secure message steganography, we carefully design a segmented message steganography algorithm in this path, which embeds the message into the medical image. Given the binary identity message $\mathbf{M} \in \{0, 1\}^L$ with a sampling length of L , we first split it into s sub-message segments. The length of i -th message segments is represented as L_i , where $\sum_{i=1}^s L_i = L$. Rather than the vanilla LSB steganography algorithm (Neeta, Snehal, and Jacobs 2006), which directly replaces the each pixel value in the LSB plane (*i.e.*, the 1-th bit planes) with the bits from the entire secret message, we replace the each binary pixel value of \mathbf{x}^i with its corresponding message segment \mathbf{M}^{L_i} . Figure 4 gives an example of the encryption and decryption process. The encryption process of our proposed segmented message steganography algorithm can be formulated by

$$\begin{aligned} \{\mathbf{Y}^i\}_{i=1}^s &= \{\mathbf{x}^i\}_{i=1}^s \dot{\mathbf{R}}_{\{L_i\}_{i=1}^s} \{\mathbf{M}^{L_i}\}_{i=1}^s, \\ \{\mathbf{B}^i\}_{i=1}^s &= \{\mathbf{x}^i\}_{i=1}^s \oplus \{\mathbf{Y}^i\}_{i=1}^s, \end{aligned} \quad (7)$$

where \mathbf{Y}^i and \mathbf{B}^i represent the i -th stego bit plane and the i -th bitmap, respectively. We define $\dot{\mathbf{R}}_{L_i}$ as a novel operation, which uses the L_i -length binary message of the segmented message \mathbf{M}^{L_i} to replace the binary value of the i -th bit plane \mathbf{x}^i element by element. When performing the replace operation, we follow the sequence from top to bottom, and within each row, from left to right. The symbol \oplus is the XOR operation. With the aid of $\{L_i\}_{i=1}^s$ and $\{\mathbf{B}^i\}_{i=1}^s$, we can recover the original message $\{\mathbf{M}^{L_i}\}_{i=1}^s$ and image $\{\mathbf{x}^i\}_{i=1}^s$, respectively:

$$\begin{aligned} \{\mathbf{M}^{L_i}\}_{i=1}^s &= \{\mathbf{Y}^i\}_{i=1}^s \dot{\mathbf{E}}_{\{L_i\}_{i=1}^s}, \\ \{\mathbf{x}^i\}_{i=1}^s &= \{\mathbf{Y}^i\}_{i=1}^s \oplus \{\mathbf{B}^i\}_{i=1}^s, \end{aligned} \quad (8)$$

where $\dot{\mathbf{E}}_{L_i}$ represents extracting L_i -length binary message from \mathbf{Y}^i . The extract sequence is also from top to bottom, and within each row, from left to right. After obtaining the stego bit planes, a learnable embedding layer with 4-convolution layers is employed to extract image embeddings. For image compression task, the embeddings of global modality are used as visual prompt, which supplies the LLM with visual information about the image. This design allows to integrate image information with the LLM’s prior knowledge, bridging the gap between image and text tasks, ultimately enhancing compression efficiency. Following (Chen et al. 2024a), we leverage the two-step lossless pixel tokenization strategy for pixel sequence semantic understanding, and the predictive distribution sampling algorithm is employed to obtain the probability distribution of each pixel from the output of LLM. With the encoded pixel values and corresponding probability distribution, we can conduct arithmetic encoder to get the bitstream. Finally, we concatenate the bitstreams from the dual-path to get the complete bitstream. The location index i ensures us to accurately recover the original dual bits.

Anatomical Priors-based Fine-Tuning

The naive LoRA fine-tuning (Hu et al. 2022) algorithm uses a random Gaussian initialization for A and zero for B , which

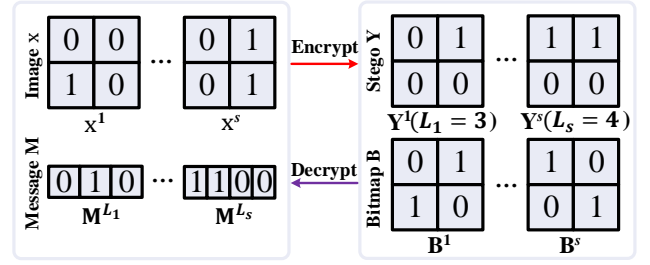


Figure 4: An example of the encryption and decryption process. We send L_1 , L_2 , L_s , and Bitmap \mathbf{B} to the receiver to ensure image \mathbf{x} and message \mathbf{M} can be losslessly recovered.

does not take into account the inherent priors (*e.g.*, the statistical properties of anatomical features) within medical images. To further enhance the compression performance and accelerate the fine-tuning process, we design a simple yet effective fine-tuning strategy, coined as anatomical priors-based fine-tuning (A-LoRA). In A-LoRA, we first use the pretrained MobileNetV3-S (Howard et al. 2019) to extract the anatomical features from medical image dataset. Then, the mean μ_f and var σ_f^2 of anatomical features are leveraged to initialize the A , *i.e.*, $A = \mathcal{N}(\mathbf{Y}^{1:s}; \mu_f, \sigma_f^2)$. This simple design guides the adaptation process of LLM in the field of medical image processing, resulting in a faster fine-tuning speed and better compression performance.

Experiments

Experimental Settings

Datasets Following (Rhee and Cho 2023), we use the Flickr2k² as the training dataset to fine-tune the LLM, where all images are uniformly center-cropped into 128×128 patches. For comprehensive evaluation of lossless compression performance, we adopt diverse medical image datasets spanning multiple modalities and anatomical regions. Detailed statistics of these datasets are provided in the [supplementary material](#).

Implementation Details In this paper, we utilize the pretrained Qwen2.5-7B³ base model as the default LLM. A-LoRA is applied to fine-tune the LLM. Similar to vanilla LoRA, the A-LoRA also approximates a large matrix by two low-rank decomposed matrices, with performance governed by rank r and the scaling factor α . We ablate the rank in some predefined values, and the alpha coefficient is twice as much as the rank for a defaulted setting. After ablation studies, we set r and α as 64, and 128, respectively (see ablation studies in the [supplementary material](#)). The local modality is then cropped into patches of size 16×16 (see ablation studies in the [supplementary material](#)), which serves as inputs to the LLM. We use the randomly but differently generated binary sequences to represent different patient identity messages \mathbf{M} . We train the entire framework using the AdamW

²<https://github.com/limbee/NTIRE2017>.

³<https://huggingface.co/Qwen/Qwen2.5-7B>.

Codec	C-19-R	C-19-C	Lung CT	Head CT	L- Spine	B-Ultra	Brain Tumor
PNG (1997)	3.10 +37.8%	4.56 +9.1%	4.32 +136.1%	3.70 +140.3%	3.53 +35.3%	3.45 +29.2%	3.52 +29.4%
JPEG2000 (2000)	2.77 +23.1%	4.47 +6.9%	4.52 +147.0%	4.66 +202.6%	4.16 +59.4%	3.01 +12.7%	3.34 +22.8%
WebP (2015)	2.79 +24.0%	4.35 +4.1%	3.52 +92.4%	3.00 +94.8%	3.30 +26.4%	3.08 +15.4%	3.27 +20.2%
FLIF (ICIP'2016)	2.59 +15.1%	4.27 +2.2%	3.36 +83.6%	2.63 +70.8%	3.14 +20.3%	2.86 +7.1%	3.15 +15.8%
JPEG-XL (2019)	2.42 +7.6%	4.34 +3.8%	3.43 +87.4%	2.61 +69.5%	3.06 +17.2%	2.85 +6.7%	3.13 +15.1%
L3C (CVPR'2019)	3.05 +35.6%	5.11 +22.3%	4.21 +130.1%	3.63 +135.7%	4.98 +90.8%	3.21 +20.2%	3.38 +24.3%
L-Infinite (CVPR'2021)	2.73 +21.3%	4.80 +14.8%	4.02 +119.7%	3.52 +128.6%	4.71 +80.5%	3.09 +15.7%	3.20 +17.6%
LC-FDNet (CVPR'2022)	2.40 +6.7%	4.27 +2.2%	3.21 +75.4%	2.39 +55.2%	2.84 +8.8%	2.78 +4.1%	2.91 +7.0%
LC-FDNet++ (CVPR'2023)	2.44 +8.4%	4.24 +1.4%	<u>1.96</u> +7.1%	<u>1.63</u> +5.8%	<u>2.75</u> +5.4%	2.83 +6.0%	<u>2.87</u> +5.5%
DLPR (TPAMI'2024)	<u>2.34</u> +4.0%	<u>4.21</u> +0.7%	3.19 +74.3%	2.27 +47.4%	2.77 +6.1%	<u>2.76</u> +3.4%	2.88 +5.9%
Delétang et al. (ICLR'2024)	3.02 +34.2%	4.48 +7.2%	4.23 +131.2%	3.31 +115.0%	3.17 +21.5%	2.93 +9.7%	3.24 +19.1%
Ours	2.25	4.18	1.83	1.54	2.64	2.67	2.72

Table 1: Compression performance of the proposed methods and other codecs in terms of bits per pixel (bpp). We show the difference in percentage to our approach, using green. The best is highlighted in bold, and the second is underlined.

optimizer (Loshchilov and Hutter 2017) with an initial learning rate of 1×10^{-4} and decreases by cosine decay learning scheduler (Loshchilov and Hutter 2016). Our method is implemented using the PyTorch framework and requires 3 days to train the entire model on 4 NVIDIA A100 GPUs.

Baseline Codecs To validate the effectiveness of our proposed method, we compare it against some comparative codecs, which can be categorized into three types: **1) Classical Codecs.** These methods rely on manually designed priors and carefully crafted frameworks. We adopt some widely used classical codecs, including PNG (Boutell 1997), JPEG2000 (Marcellin et al. 2000), WebP (Si and Shen 2015), FLIF (Sneyers and Wuille 2016), and JPEG-XL (Alakuijala et al. 2019). **2) Learned Image Compression (LIC).** LIC models typically optimize the rate-distortion trade-off directly through deep neural network architectures. Representative LIC models include: L3C (Mentzer et al. 2019), L-Infinite (Bai et al. 2021), LC-FDNet (Rhee et al. 2022), LC-FDNet++ (Rhee and Cho 2023) and DLPR (Bai et al. 2024). **3) LLM-based Compressor.** We also reproduce the LLM-based lossless image codec proposed by Delétang et al. (Delétang et al. 2024) in our experiments. Since the LLM used in their approach is not open-source, we substitute it with Qwen2.5-7B as the default model while following their other settings.

Metrics In this study, we utilize bits per pixel (bpp) as the metric for evaluating compression ratios. This metric is calculated by dividing the total number of bits in the compressed file by the total number of pixels in the original image. For bpp, the lower, the better.

Experimental Results

Model Performance As shown in Table 1, our proposed method achieves the new state-of-the-art (SOTA) compression performance compared to previous methods. Specifically, it outperforms all other methods in seven medical image datasets across multiple imaging modalities, including CT, MRI and ultrasonoscopy. On the C-19-R and L-Spine datasets, our approach further reduces file size by

7.6%-17.2% compared to the best classical codec, JPEG-XL. When compared to SOTA LIC codecs such as L3C and DLPR, our approach also demonstrates superior results. For example, the bpp of DLPR is 2.34, while our method achieves 2.25, reflecting 4.0% improvement. Additionally, in comparison with a LLM-based codec, our method reduces the bpp from 3.02 to 2.25 on the C-19-R dataset. These results underscore how our architecture, enhanced with dual-path compression and A-LoRA significantly improves the performance in the lossless image compression task.

Runtime and LLM Size We present the encoding and decoding speed for some competitive methods on the C-19-R dataset in Table 2. The encoding and decoding time are dramatically decreasing compared to the LLM-based codec (Delétang et al. 2024). This phenomenon is attributed to the dual-path compression scheme, where LLMs only need to compress the local modality. Compared to other codecs, our method (1.5B) also renders a competitive inference speed while maintaining the SOTA compression performance. Furthermore, we conduct experiments utilizing three Qwen models with varying parameters to evaluate the impact of LLM size on compression performance. The results indicate that the degradation of compression performance is not prominent as the model size decreases, *i.e.*, smaller models can still achieve acceptable performance.

Security Validation and Visualization of Stego Images

As shown in Figure 5, our proposed segmented message steganography algorithm achieves a remarkable invisibility to human observers, as the visual fidelity metrics are excellent, *e.g.*, PSNR of 68.79 dB (very high - above 40 dB is considered excellent), and SSIM of 0.999998 (nearly perfect structural similarity) (Kaissis et al. 2020). Meanwhile, only 292 pixels out of 82,928 total pixels are changed (0.3521% change ratio), indicating efficient embedding with minimal alterations. The histogram of pixel difference distribution has a very high peak at 0, indicating that most of the pixels have not been modified.

Codec	Bpp ↓	Params.	Enc. Time	Dec. Time
JPEG-XL	2.42	—	0.79s	0.12s
L3C	3.05	5M	8.21s	7.91s
LC-FDNet	2.40	23.70M	1.60s	1.60s
DLPR	2.34	22.2M	1.53s	2.07s
Deletang et al.	3.02	8B	10.47s	287.30s
Ours (1.5B)	2.25	1.5B+2M	1.55s	39.91s
Ours (3B)	2.27	3B+3M	3.21s	64.30s
Ours (7B)	2.25	7B+4M	6.37s	141.60s

Table 2: Runtime analysis and LLM size analysis on the C-19-R dataset. 8 NVIDIA A100 GPUs (#batch_size:16, #sub-progress: 2 per GPU) for parallel processing.

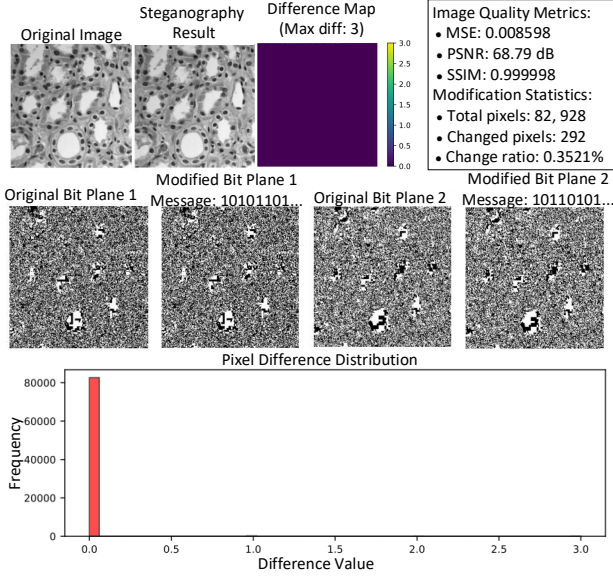


Figure 5: Visualization of stego images. The proposed segmented message steganography algorithm achieves an invisible message encryption.

Ablation Studies

To further analyze our architecture, we conduct ablation studies on the C-19-R dataset.

Visual Prompt and A-LoRA We begin by establishing a baseline model where LLM is fixed, without the use of visual prompts. Table 3 shows that employing the embeddings of global modality as visual prompts reduces the bpp from 3.34 to 2.77, underscoring the effectiveness of visual prompts in bridging the gap between the textual prior within LLM and image compression tasks. After applying the LoRA fine-tuning, our visual prompts continue to achieve a performance gain of bpp. As shown in Figure 6, it is evident that utilizing A-LoRA fine-tuning strategy rather than vanilla LoRA further improves the compression performance and accelerates the training speed.

Choice of Retention hyperparameter β The retention hyperparameter β controls the proportion of information al-

Baseline	Visual Prompt	LoRA	A-LoRA	Bpp ↓
✓	✗	✗	✗	3.34
✓	✓	✗	✗	2.77
✓	✓	✓	✗	2.40
✓	✓	✗	✓	2.25

Table 3: Component ablation experimental results on the C-19-R dataset, using bpp as the metric.

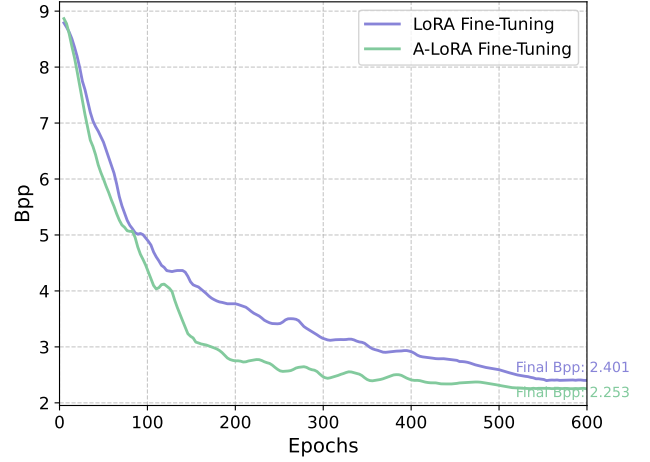


Figure 6: The bpp score tendency of our method with different fine-tuning strategy during the training period.

located to global modalities during the adaptive modalities decomposition process. To determine its optimal value, we conducted experiments on the C-19-R dataset, evaluating the compression performance for $\beta \in \{0.6, 0.7, 0.8, 0.9\}$. The results are presented in Table 4. The results demonstrate that $\beta = 0.8$ provides the optimal trade-off between global and local information retention, achieving the best compression performance. Smaller values of β (e.g., 0.6, 0.7) underutilize global information, while larger value (e.g., 0.9) compromises the effectiveness of local modality compression. Therefore, we set $\beta = 0.8$ as the default value in our method.

β	0.6	0.7	0.8	0.9
Bpp ↓	2.52	2.41	2.25	2.38

Table 4: Impact of β on Compression Performance.

Conclusion

In this paper, we propose the joint lossless compression and steganography framework, which ensures the security for compressing medical images. Under this framework, the adaptive modalities decomposition strategy is first designed to explicitly decompose images into global and local modalities. Then, we present a dual-path compression scheme, which takes the first attempt to deploy LLMs' unprece-

dented intelligence for arithmetic coding in the combined paradigm. Combined with the carefully designed anatomical priors-based low-rank adaptation (A-LoRA) fine-tuning strategy, our method achieves superior compression performance against other SOTA codecs with comparable inference time. As this framework is still in its early stages, future works could focus on developing more lightweight LLMs for compression, which makes it feasible to deploy the method in resource-constrained medical scenarios.

References

- Alakuijala, J.; Van Asseldonk, R.; Boukourt, S.; Bruse, M.; Comşa, I.-M.; Firsching, M.; Fischbacher, T.; Kliuchnikov, E.; Gomez, S.; Obryk, R.; et al. 2019. JPEG XL next-generation image compression architecture and coding tools. In *Applications of digital image processing XLII*, volume 11137, 112–124. SPIE.
- An, H.; Chen, Y.; Sun, Z.; and Li, X. 2024. SentenceVAE: Enable Next-sentence Prediction for Large Language Models with Faster Speed, Higher Accuracy and Longer Context. *arXiv preprint arXiv:2408.00655*.
- Bai, Y.; Liu, X.; Wang, K.; Ji, X.; Wu, X.; and Gao, W. 2024. Deep Lossy Plus Residual Coding for Lossless and Near-Lossless Image Compression. *IEEE Transactions on Pattern Analysis and Machine Intelligence*, 46(5): 3577–3594.
- Bai, Y.; Liu, X.; Zuo, W.; Wang, Y.; and Ji, X. 2021. Learning Scalable ℓ_∞ -constrained Near-lossless Image Compression via Joint Lossy Image and Residual Compression. In *IEEE/CVF Conference on Computer Vision and Pattern Recognition (CVPR)*.
- Boutell, T. 1997. PNG (Portable Network Graphics) Specification Version 1.0. Technical report, W3C.
- Cai, S.; Chen, L.; Zhong, S.; Yan, L.; Zhou, J.; and Zou, X. 2024. Make lossy compression meaningful for low-light images. In *Proceedings of the AAAI Conference on Artificial Intelligence*, volume 38, 8236–8245.
- Chen, K.; Zhang, P.; Liu, H.; Liu, J.; Liu, Y.; Huang, J.; Wang, S.; Yan, H.; and Li, H. 2024a. Large Language Models for Lossless Image Compression: Next-Pixel Prediction in Language Space is All You Need. *arXiv:2411.12448*.
- Chen, K.; Zhang, P.; Qin, T.; Wang, S.; Yan, H.; and Li, H. 2024b. Test-time adaptation for image compression with distribution regularization. *arXiv:2410.12191*.
- Child, R. 2021. Very Deep VAEs Generalize Autoregressive Models and Can Outperform Them on Images. *arXiv:2011.10650*.
- Delétang, G.; Ruoss, A.; Duquenne, P.; Catt, E.; Genewein, T.; Mattern, C.; Grau-Moya, J.; Wenliang, L. K.; Aitchison, M.; Orseau, L.; Hutter, M.; and Veness, J. 2024. Language Modeling Is Compression. In *ICLR*.
- Du, J.; Zhou, C.; Cao, N.; Chen, G.; Chen, Y.; Cheng, Z.; Song, L.; Lu, G.; and Zhang, W. 2025. Large Language Model for Lossless Image Compression with Visual Prompts. *arXiv:2502.16163*.
- Gou, C.; Felemban, A.; Khan, F. F.; Zhu, D.; Cai, J.; Rezatofighi, H.; and Elhoseiny, M. 2024. How Well Can Vision Language Models See Image Details? *arXiv preprint arXiv:2408.03940*.
- Heurtel-Depeiges, D.; Ruoss, A.; Veness, J.; and Genewein, T. 2024. Compression via pre-trained transformers: A study on byte-level multimodal data. *arXiv preprint arXiv:2410.05078*.
- Howard, A.; Sandler, M.; Chu, G.; Chen, L.-C.; Chen, B.; Tan, M.; Wang, W.; Zhu, Y.; Pang, R.; Vasudevan, V.; et al. 2019. Searching for mobilenetv3. In *Proceedings of the IEEE/CVF international conference on computer vision*, 1314–1324.
- Hu, E. J.; Shen, Y.; Wallis, P.; Allen-Zhu, Z.; Li, Y.; Wang, S.; Wang, L.; Chen, W.; et al. 2022. Lora: Low-rank adaptation of large language models. *ICLR*, 1(2): 3.
- Huang, Y.; Zhang, J.; Shan, Z.; and He, J. 2024. Compression represents intelligence linearly. *arXiv preprint arXiv:2404.09937*.
- Jia, Z.; Li, J.; Li, B.; Li, H.; and Lu, Y. 2024. Generative Latent Coding for Ultra-Low Bitrate Image Compression. In *Proceedings of the IEEE/CVF Conference on Computer Vision and Pattern Recognition (CVPR)*, 26088–26098.
- Kaissis, G. A.; Makowski, M. R.; Rückert, D.; and Braren, R. F. 2020. Secure, privacy-preserving and federated machine learning in medical imaging. *Nature Machine Intelligence*, 2(6): 305–311.
- Kang, N.; Qiu, S.; Zhang, S.; Li, Z.; and Xia, S.-T. 2022. Pilc: Practical image lossless compression with an end-to-end gpu oriented neural framework. In *Proceedings of the IEEE/CVF Conference on Computer Vision and Pattern Recognition*, 3739–3748.
- Li, D.; Bai, Y.; Wang, K.; Jiang, J.; Liu, X.; and Gao, W. 2025. CALLIC: Content Adaptive Learning for Lossless Image Compression. In *Proceedings of the AAAI Conference on Artificial Intelligence*, volume 39, 4679–4688.
- Liu, X.; Wang, M.; Wang, S.; and Kwong, S. 2024. Bilateral Context Modeling for Residual Coding in Lossless 3D Medical Image Compression. *IEEE Transactions on Image Processing*, 33: 2502–2513.
- Loshchilov, I.; and Hutter, F. 2016. Sgdr: Stochastic gradient descent with warm restarts. *arXiv preprint arXiv:1608.03983*.
- Loshchilov, I.; and Hutter, F. 2017. Decoupled weight decay regularization. *arXiv preprint arXiv:1711.05101*.
- Lu, J.; Zhang, L.; Zhou, X.; Li, M.; Li, W.; and Gu, S. 2025. Learned Image Compression with Dictionary-based Entropy Model. In *Proceedings of the Computer Vision and Pattern Recognition Conference (CVPR)*, 12850–12859.
- MacKay, D. J. 2003. *Information theory, inference and learning algorithms*. Cambridge university press.
- Mao, Y.; Pirk, H.; and Xue, C. J. 2025. Lossless Compression of Large Language Model-Generated Text via Next-Token Prediction. *arXiv preprint arXiv:2505.06297*.
- Mao, Y.; Wang, J.; Guan, N.; and Xue, C. J. 2025. WISE: A Framework for Gigapixel Whole-Slide-Image Lossless Compression. In *Proceedings of the Computer Vision and Pattern Recognition Conference (CVPR)*, 29342–29351.

- Marcellin, M. W.; Gormish, M. J.; Bilgin, A.; and Boliek, M. P. 2000. An overview of JPEG-2000. In *Proceedings DCC 2000. Data compression conference*, 523–541. IEEE.
- Mentzer, F.; Agustsson, E.; Tschannen, M.; Timofte, R.; and Gool, L. V. 2019. Practical full resolution learned lossless image compression. In *Proceedings of the IEEE/CVF conference on computer vision and pattern recognition*, 10629–10638.
- Neeta, D.; Snehal, K.; and Jacobs, D. 2006. Implementation of LSB steganography and its evaluation for various bits. In *2006 1st international conference on digital information management*, 173–178. IEEE.
- Pinheiro Cinelli, L.; Araújo Marins, M.; Barros da Silva, E. A.; and Lima Netto, S. 2021. *Variational Autoencoder*, 111–149. Cham: Springer International Publishing. ISBN 978-3-030-70679-1.
- Rhee, H.; and Cho, N. I. 2023. Lossless Compression of Raw Images by Learning the Prediction and Frequency Decomposition. In *2023 IEEE International Conference on Visual Communications and Image Processing (VCIP)*, 1–5.
- Rhee, H.; Jang, Y. I.; Kim, S.; and Cho, N. I. 2022. LC-FDNet: Learned Lossless Image Compression with Frequency Decomposition Network. In *2022 IEEE/CVF Conference on Computer Vision and Pattern Recognition (CVPR)*, 6023–6032.
- Schirrmester, R.; Zhou, Y.; Ball, T.; and Zhang, D. 2020. Understanding anomaly detection with deep invertible networks through hierarchies of distributions and features. *Advances in Neural Information Processing Systems*, 33: 21038–21049.
- Shannon, C. E. 1948. A mathematical theory of communication. *The Bell system technical journal*, 27(3): 379–423.
- Si, Z.; and Shen, K. 2015. Research on the WebP image format. In *Advanced graphic communications, packaging technology and materials*, 271–277. Springer.
- Sneyers, J.; and Wuille, P. 2016. FLIF: Free lossless image format based on MANIAC compression. In *2016 IEEE international conference on image processing (ICIP)*, 66–70. IEEE.
- Sugiyama, H.; Suzuki, K.; and Matsuda, I. 2024. Initial bits generation for lossless image compression using bits-back coding with a latent variable model. In *International Workshop on Advanced Imaging Technology (IWAIT) 2024*, volume 13164, 551–555. SPIE.
- Tang, Z.; Song, J.; Zhang, X.; and Sun, R. 2016. Multiple-image encryption with bit-plane decomposition and chaotic maps. *Optics and Lasers in Engineering*, 80: 1–11.
- Tian, K.; Jiang, Y.; Yuan, Z.; Peng, B.; and Wang, L. 2024. Visual Autoregressive Modeling: Scalable Image Generation via Next-Scale Prediction. *arXiv preprint arXiv:2404.02905*.
- Valmeekam, C. S. K.; Narayanan, K.; Kalathil, D.; Chamberland, J.-F.; and Shakkottai, S. 2023. LLMZip: Lossless Text Compression using Large Language Models. *arXiv preprint arXiv:2306.04050*.
- Varma, D. R. 2012. Managing DICOM images: Tips and tricks for the radiologist. *Indian Journal of Radiology and Imaging*, 22(01): 4–13.
- Wang, J.; Li, Q.; Zheng, P.; Pu, X.; and Ren, Y. 2025. ChronoSelect: Robust Learning with Noisy Labels via Dynamics Temporal Memory. *arXiv preprint arXiv:2507.18183*.
- Yamamoto, H. 1994. Coding theorems for Shannon’s cipher system with correlated source outputs, and common information. *IEEE Transactions on Information Theory*, 40(1): 85–95.
- Yang, S.; Qu, T.; Lai, X.; Tian, Z.; Peng, B.; Liu, S.; and Jia, J. 2023. An improved baseline for reasoning segmentation with large language model. *CoRR*.
- Zhang, Y.; Zheng, P.; Jiang, J.; Xiao, P.; and Gao, X. 2023. FCIR: Rethink aerial image super resolution with Fourier analysis. In *ICASSP 2023-2023 IEEE International Conference on Acoustics, Speech and Signal Processing (ICASSP)*, 1–5. IEEE.
- Zhang, Y.; Zheng, P.; Zeng, C.; Xiao, B.; Li, Z.; and Gao, X. 2024a. Jointly RS Image Deblurring and Super-Resolution With Adjustable-Kernel and Multi-Domain Attention. *IEEE Transactions on Geoscience and Remote Sensing*.
- Zhang, Z.; Wang, H.; Chen, Z.; and Liu, S. 2024b. Learned Lossless Image Compression based on Bit Plane Slicing. In *Proceedings of the IEEE/CVF Conference on Computer Vision and Pattern Recognition (CVPR)*, 27579–27588.
- Zheng, H.; and Gao, W. 2024. End-to-end rgb-d image compression via exploiting channel-modality redundancy. In *Proceedings of the AAAI Conference on Artificial Intelligence*, volume 38, 7562–7570.
- Zheng, P.; Chen, K.; Huang, J.; Chen, B.; Liu, J.; Ren, Y.; and Pu, X. 2025. Efficient Medical Image Restoration via Reliability Guided Learning in Frequency Domain. *arXiv preprint arXiv:2504.11286*.
- Zheng, P.; Jiang, J.; Zhang, Y.; Zeng, C.; Qin, C.; and Li, Z. 2023. CGC-net: A context-guided constrained network for remote-sensing image super resolution. *Remote Sensing*, 15(12): 3171.
- Zhou, L.; Cai, C.; Gao, Y.; Su, S.; and Wu, J. 2018. Variational Autoencoder for Low Bit-rate Image Compression. In *Proceedings of the IEEE Conference on Computer Vision and Pattern Recognition (CVPR) Workshops*.

Appendix

Supplementary Material for Adaptive Modalities Decomposition

Proof. Why $I(\mathbf{x}; \mathbf{x})$ equals to $H(\mathbf{x})$?

Proof. In information theory, the mutual information $I(\mathbf{x}; \mathbf{y})$ between two discrete random variables \mathbf{x} and \mathbf{y} is defined as:

$$I(\mathbf{x}; \mathbf{y}) = \sum_{x \in \mathcal{X}} \sum_{y \in \mathcal{Y}} p(x, y) \log \frac{p(x, y)}{p(x)p(y)} \quad (9)$$

Dataset	Description	# Num.	Avg. Resolution
Flickr2k*	Natural	2650	2048×1024
C-19-R†	Chest X-ray	42300	300×300
C-19-C†	Lung CT	262	512×512
Lung CT†	Lung CT	7944	1024×768
Head CT†	Head CT	200	640×480
L-Spine†	Spine CT	2477	256×256
B-Ultra†	Ultrasound	1578	640×480
Brain Tumor†	Brain MRI	7022	512×512

Table 5: Datasets introduction. * and † indicate training and testing datasets, respectively. C-19-R and C-19-C refer to the COVID-19 radiograph dataset, and COVID-19 CT scan dataset, respectively. L-Spine is the Lumbar Spine dataset. B-Ultra refers to the Breast Ultrasound dataset.

When $\mathbf{y} = \mathbf{x}$, the joint distribution $p(x, x)$ degrades to $p(x)$, and the conditional probability $p(x|x) = 1$. Substituting these into the mutual information definition:

$$\begin{aligned}
I(\mathbf{x}; \mathbf{x}) &= \sum_{x \in \mathcal{X}} p(x) \log \frac{p(x)}{p(x)p(x)} \\
&= \sum_{x \in \mathcal{X}} p(x) \log \frac{1}{p(x)} \\
&= H(\mathbf{x})
\end{aligned} \tag{10}$$

where $H(\mathbf{x}) = -\sum_{x \in \mathcal{X}} p(x) \log p(x)$ is the entropy of \mathbf{x} . This equality holds because the self-information $\log \frac{1}{p(x)}$ exactly corresponds to the contribution of each outcome to the entropy. Therefore, the mutual information between a random variable and itself equals its entropy, representing the total information content. This fundamental property is utilized in the paper’s adaptive modalities decomposition to quantify and partition the image information. \square

Moreover, we provide pseudocode, Algorithm 1 and Algorithm 2 for each method bit plane slicing and adaptive modalities decomposition, respectively.

Algorithm 1 Bit Plane Slicing Algorithm

```

1: Input: image (tensor), bits (integer)
2: Output: bit_planes (list)
3: function BIT_SLICING(image, bits)
4:   bit_planes ← [] ▷ Initialize an empty list
5:   for  $i = 0$  to bits - 1 do
6:     bit_planes.append(image % 2)
7:     image ← image // 2 ▷ Integer division by 2
8:   end for
9:   return bit_planes ▷ Return bit-planes
10: end function

```

Dataset Description

Here, we provide the detailed information of the training dataset and testing datasets, including their modalities, number of samples, and image resolutions in Table 5.

Algorithm 2 Adaptive Modalities Decomposition Algorithm

```

1: Input: image  $\mathbf{x}$  (tensor),  $\beta$  (integer), mutual information score function  $\mathcal{I}(\cdot)$ 
2: Output: global modality  $\mathbf{x}^{1:s}$ , local modality  $\mathbf{x}^{s+1:8}$ 
3: Initialize: cumulative mutual information amount:  $T_{cu} \leftarrow 0$ , whole information amount in the image:  $T_w \leftarrow \mathcal{I}(\mathbf{x}; \mathbf{x})$ , target retentive information amount:  $T_t \leftarrow \beta * T_w$ 
4: for  $s = 1$  to 8 do
5:   step 1: calculate the information amount in the current bit plane:  $T_c \leftarrow \mathcal{I}(\mathbf{x}^s; \mathbf{x})$ 
6:   step 2: update  $T_{cu} \leftarrow T_{cu} + T_c$ 
7:   if  $T_{cu} \geq T_t$  then break
8: end for
9: return  $\mathbf{x}^{1:s}, \mathbf{x}^{s+1:8}$ 

```

Rank r	Alpha	Bpp ↓	Gain
8	16	2.30	+2.2%
16	32	2.29	+1.78%
32	64	2.27	+0.89%
64	128	2.25	—
128	256	2.26	+0.44%

Table 6: Ablation experiments for A-LoRA, test results on the C-19-R dataset, using bpp as metric.

Different Rank r for A-LoRA

The rank and corresponding alpha coefficient in A-LoRA would significantly affect the compression performance. As shown in Table 6, we ablate the rank in some predefined values, and alpha is twice as much as the rank for a defaulted setting. Theoretically, larger rank leads to more powerful representation ability, resulting in better compression ratios. However, as shown in Table 6, the compression performance remains essentially unchanged as the rank increases beyond a certain point. To strike a great balance between performance and efficiency, we set the rank and alpha to 64 and 128, respectively.

Patch Size

The patch size determines the context length of LLM, which can affect the compression performance. Table 7 reveals that moderate patch size *i.e.*, 16×16 achieves the optimal performance, as short-context length provides limited contextual information for LLM while long-context impairs the performance due to the degradation of position embeddings.

Patch Size	8×8	12×12	16×16	24×24	32×32
Bpp ↓	2.74	2.47	2.25	2.32	2.91

Table 7: Comparison of different patch sizes for LLM. Moderate patch size is the best.

Reproducibility Checklist

Unless specified otherwise, please answer “yes” to each question if the relevant information is described either in the paper itself or in a technical appendix with an explicit reference from the main paper. If you wish to explain an answer further, please do so in a section titled “Reproducibility Checklist” at the end of the technical appendix.

This paper:

- Includes a conceptual outline and/or pseudocode description of AI methods introduced **(yes)**
- Clearly delineates statements that are opinions, hypothesis, and speculation from objective facts and results **(yes)**
- Provides well marked pedagogical references for less-familiar readers to gain background necessary to replicate the paper **(yes)**

Does this paper make theoretical contributions? **(yes)**

- All assumptions and restrictions are stated clearly and formally. **(yes)**
- All novel claims are stated formally (e.g., in theorem statements). **(yes)**
- Proofs of all novel claims are included. **(yes)**
- Proof sketches or intuitions are given for complex and/or novel results. **(yes)**
- Appropriate citations to theoretical tools used are given. **(yes)**
- All theoretical claims are demonstrated empirically to hold. **(yes)**
- All experimental code used to eliminate or disprove claims is included. **(yes)**

Does this paper rely on one or more datasets? **(yes)**

- A motivation is given for why the experiments are conducted on the selected datasets **(yes)**
- All novel datasets introduced in this paper are included in a data appendix. **(yes)**
- All novel datasets introduced in this paper will be made publicly available upon publication of the paper with a license that allows free usage for research purposes. **(yes)**
- All datasets drawn from the existing literature (potentially including authors’ own previously published work) are accompanied by appropriate citations. **(yes)**
- All datasets drawn from the existing literature (potentially including authors’ own previously published work) are publicly available. **(yes)**
- All datasets that are not publicly available are described in detail, with explanation why publicly available alternatives are not scientifically satisfying. **(yes)**

Does this paper include computational experiments? **(yes)**

- This paper states the number and range of values tried per (hyper-) parameter during development of the paper, along with the criterion used for selecting the final parameter setting. **(yes)**
- Any code required for pre-processing data is included in the appendix. **(yes)**

- All source code required for conducting and analyzing the experiments is included in a code appendix. **(yes)**
- All source code required for conducting and analyzing the experiments will be made publicly available upon publication of the paper with a license that allows free usage for research purposes. **(yes)**
- All source code implementing new methods have comments detailing the implementation, with references to the paper where each step comes from **(yes)**
- If an algorithm depends on randomness, then the method used for setting seeds is described in a way sufficient to allow replication of results. **(yes)**
- This paper specifies the computing infrastructure used for running experiments (hardware and software), including GPU/CPU models; amount of memory; operating system; names and versions of relevant software libraries and frameworks. **(yes)**
- This paper formally describes evaluation metrics used and explains the motivation for choosing these metrics. **(yes)**
- This paper states the number of algorithm runs used to compute each reported result. **(yes)**
- Analysis of experiments goes beyond single-dimensional summaries of performance (e.g., average; median) to include measures of variation, confidence, or other distributional information. **(no)**
- The significance of any improvement or decrease in performance is judged using appropriate statistical tests (e.g., Wilcoxon signed-rank). **(yes)**
- This paper lists all final (hyper-)parameters used for each model/algorithm in the paper’s experiments. **(partial)**